

# On Buggy Resizing Libraries and Surprising Subtleties in FID Calculation

Gaurav Parmar<sup>1</sup>   Richard Zhang<sup>2</sup>   Jun-Yan Zhu<sup>1</sup>  
<sup>1</sup>Carnegie Mellon University   <sup>2</sup>Adobe Research

## Abstract

We investigate the sensitivity of the Fréchet Inception Distance (FID) score to inconsistent and often incorrect implementations across different image processing libraries. FID score is widely used to evaluate generative models, but each FID implementation uses a different low-level image processing process. Image resizing functions in commonly-used deep learning libraries often introduce aliasing artifacts. We observe that numerous subtle choices need to be made for FID calculation and a lack of consistencies in these choices can lead to vastly different FID scores. In particular, we show that the following choices are significant: (1) selecting what image resizing library to use, (2) choosing what interpolation kernel to use, (3) what encoding to use when representing images. We additionally outline numerous common pitfalls that should be avoided and provide recommendations for computing the FID score accurately. We provide an easy-to-use optimized implementation of our proposed recommendations in the accompanying code.

## 1. Introduction

The Fréchet Inception Distance (FID) metric [23] is ubiquitously used to evaluate generative models [23, 28, 8, 46, 30]. Under the hood, computing FID contains several subtle implementation decisions, notably image resizing, quantization, and formatting. While seemingly innocuous, we find these choices actually have a large effect on the final score. Consider Figure 1, given the same input image, different image processing libraries produce drastically different results, most of which are incorrect and contain aliasing artifacts due to improper filtering implementations.

However, researchers have used separate protocols, including different resizing libraries, image formats, quantization when computing FID scores. This makes comparisons across papers extremely difficult. The reported FID scores often become only meaningful within the same paper. However, it is not always feasible to repeat the experiments from other papers, and it is a common practice to copy and paste the FID scores without re-computing them. This can be problematic as the scores being compared together may, in

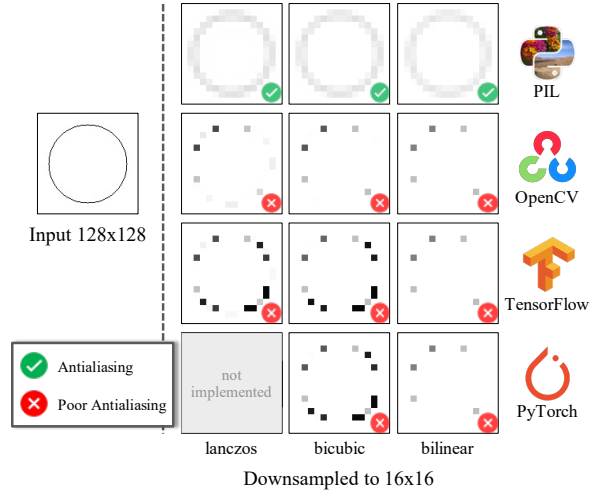


Figure 1: **Downsampling a circle.** We Resize an input image of a circle (left) by a factor of 8 using different commonly used methods with different image processing libraries. The Lanczos, bicubic and bilinear implementations by PIL (top row) antialias correctly (marked as ✓). The other implementations introduce aliasing artifacts (marked as ✗). Many evaluation metrics of generative models such as Fréchet Inception Distance [23] use the downsampling function.

fact, use different protocols.

We identify that the core issue here is the resizing operation. As shown in Figure 1, image resizing functions in widely-used deep learning libraries (such as TensorFlow and PyTorch) often produce results with severe aliasing artifacts, as their implementations do not follow the correct filtering steps taught in standard computer vision and signal processing textbooks and lectures. Additionally, our experiments show that both image compression and quantization have a large effect on FID scores, while the results barely affect human perception and image assessment metrics such as PSNR and LPIPS [58].

We discuss some common pitfalls encountered when computing the FID scores and mention various ways of avoiding them. For example, people training models on low-resolution images (128 or 256) due to limited computational resources may use different resizing libraries and image formats to prepare the dataset images. This introduces a whole new level of subtleties to model comparisons at low-res images. To ad-

dress the above issues, we recommend a standardized protocol, and provide an easy-to-use FID evaluation library, `clean-fid` ([github.com/GaParmar/clean-fid](https://github.com/GaParmar/clean-fid)). The take-home message is that we need to pay attention to low-level image processing when training and evaluating generative models such as GANs. We show that the same differences apply to other generative model evaluation metrics such as KID [5] as this metric also involves the same type of image processing steps. More details and results can be found on our [website](#).

## 2. Related Works

**Deep generative models.** A wide range of image and video synthesis applications [61, 41, 34, 51] have been enabled, as a result of tremendous progress in deep generative models such as GANs [22, 44, 26, 28, 9], VAEs [31, 46, 42], autoregressive models [39], flow-based models [14, 30], and energy-based models [48, 38, 17]. It is often relatively easier to evaluate individual model’s performance on downstream computer vision and graphics tasks, as these tasks have a clear target for a given input. However, evaluating unconditional generative models remains an open problem. It is still an important goal, as most generative models are not tailored to any downstream task.

**Evaluating generative models.** The community has introduced many evaluation protocols. One idea is to conduct user studies on cloud-sourcing platforms for either assessing the samples’ image quality [13, 49, 60] or identifying duplicate images [4]. Due to the subtle differences in user study protocols (e.g., UI design, fees, date/time), it is difficult to replicate results across different papers. Large-scale user studies can also be expensive, prohibiting its usage when evaluating hundreds of model variants and checkpoints during the development stage. Several works evaluate the generative model from a self-supervised feature learning perspective, by repurposing the learned discriminators [44] or accompanying encoders [15] for a different, image classification task. However, the representation power of the discriminator or encoder does not directly reflect the generators’ sample quality and diversity. In addition, not every generative model is trained with a discriminator or encoder.

To overcome the previous issues, an area of focus is automatic metrics that directly assess the samples of generative models. Various metrics been proposed, criticized, and modified. Commonly-used ones include log-likelihood [31, 22], density estimate with Parzen window [22], Inception Score [49], Perceptual Path Length [28], Fréchet Inception Distance (FID) [23], Classification Accuracy Score and its early variants [45, 49], Classifier Two-sample Tests [33, 36], precision and recall [47, 32], Kernel Inception Distance (KID) [5], among others. Each metric has associated pros and cons [54, 6] and none are perfect.

Among them, Fréchet Inception Distance (FID) has become the most widely-used metrics, as it can model intra-class diversity better than Inception Score, is easy and fast to compute, without training additional classifiers [45], and has been shown to be consistent with human perception [23]. As a result, it has been used in recent GANs papers [56, 28, 9] as well as large-scale evaluation study [37], despite facing criticism about the fact that FID is a biased estimator and sensitive to the number of samples used in the evaluation [10]. Our goal here is *not* to study which one is a better metric. Instead, we focus our study on the popular FID metric and how subtle details and buggy image resizing functions can affect the final scores. Note that the resizing and quantization operations we study in detail are applicable to all generative model development and any metric that contains such operations.

## 3. Preliminaries

In this section, we discuss several low-level image processing steps using different popular libraries. We find that many of these details can have a large effect on the FID score being computed. Figure 2 details the step-by-step process for both dataset preparation and model evaluations.

### 3.1. FID Calculation

The Fréchet Inception Distance (FID) score aims to measure the gap between two data distributions [23], such as between a training set and samples from a generator.

**Dataset pre-processing.** We denote the original real image distribution as  $\mathbf{x} \sim p_{\text{data}}(\mathbf{x})$ , where  $x \in \mathbb{Z}^{H \times W \times 3}$ . Note that images are saved as 8-bit integers, represented by  $\mathbb{Z}$ . Training and developing large-scale GANs at the original resolution [9, 28] is often prohibitively expensive, and it requires tens or even hundreds of models during development. As such, developing on lower-resolution versions of the original dataset is common practice [35, 59, 57], such as  $1024 \rightarrow 256$  on FFHQ or  $256 \rightarrow 128$  on ImageNet.

As shown in the top branch of Figure 2, to prepare a lower-resolution training set, one must downsample using a resize function  $\psi_{\text{data}}$ . Note that downsampling should involve an antialiasing step, which can convert integers into a floating point number,  $\mathbb{Z} \rightarrow \mathbb{R}$ . A quantization step is typically added afterwards to cast back to  $\mathbb{Z}$ , so that images can be potentially saved to disk. This data preparation step introduces a new data distribution of low-res real images:  $\bar{\mathbf{x}} \sim p_{\text{data}}(\bar{\mathbf{x}})$ , where  $\bar{\mathbf{x}} \in \mathbb{Z}^{\bar{H} \times \bar{W} \times 3}$ .

**Evaluating a generator.** A generator  $G$  that learns to map a latent code  $\mathbf{z} \in \mathcal{N}(0, I)$  to output images  $G(\mathbf{z}) \in \mathbb{R}^{\bar{H} \times \bar{W} \times 3}$  is trained on the lower resolution dataset.

A common method of evaluating the generator is passing both real and generated images through a feature extractor  $\mathcal{F}$ , fitting a Gaussian distribution, and measuring the Fréchet

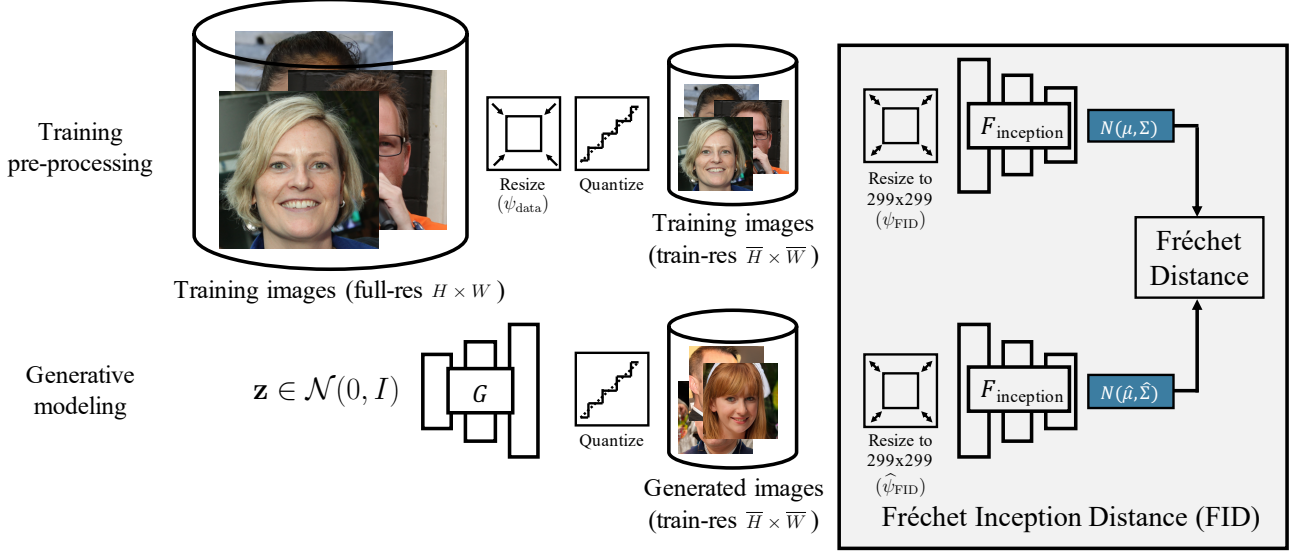


Figure 2: **Overview of the steps involved in FID.** Generative modeling and evaluation require several subtleties in image pre-processing. **Top:** First, the image dataset may come with higher resolutions than the model training (e.g., 1024 for the FFHQ dataset used at 256 resolution). Training set pre-processing requires a resize and possibly quantization. **Bottom:** While the output of a generator  $G(z)$  is a floating-point value (approximately continuous), images are typically saved as an unsigned 8-bit integer, resulting in a quantization. FID aims to measure how well generative model  $G(z)$  mimics this training distribution. The calculation resizes the image into  $299 \times 299$  resolution, fits Gaussians in the Inception network’s [52] feature space, and takes the Fréchet distance between two distributions. We study the effects of the resize and quantization steps, which have a nontrivial effect on the final metric.

distance between the two distributions. Deep network activations have been shown to correspond well with human perceptual judgments [58] and are often used as training objectives [20, 24, 16]. The feature extractor  $\mathcal{F}$  used for this task is an InceptionV3 model [52]. Because this model is trained on  $299 \times 299 \times 3$  ImageNet image crops [12], the training and generated images are resized using resizing functions  $\psi_{\text{FID}}$  and  $\hat{\psi}_{\text{FID}}$ , respectively, before being processed. Note that we also have to quantize an image to 8 bit unsigned integer values and sometimes save the image to disk with different image compression options. These operations are represented by  $Q$  for reference images  $\mathbf{x}$  and by  $\hat{Q}$  for synthesized images  $G(\mathbf{z})$ .

$$\mathbf{f} = \mathcal{F}(\psi_{\text{FID}}(Q(\psi_{\text{data}}(\mathbf{x})))), \quad (1)$$

$$\hat{\mathbf{f}} = \mathcal{F}(\hat{\psi}_{\text{FID}}(\hat{Q}(G(\mathbf{z}))))). \quad (2)$$

After the images are appropriately resized and the features are extracted, the mean  $(\mu, \hat{\mu})$  and covariance matrix  $(\Sigma, \hat{\Sigma})$  of the corresponding set of features  $\mathbf{f}$  and  $\hat{\mathbf{f}}$  are used to compute the Fréchet distance shown in the equation below.

$$\text{FID} = \|\mu - \hat{\mu}\|_2^2 + \text{Tr}(\Sigma + \hat{\Sigma} - 2(\Sigma\hat{\Sigma})^{1/2}), \quad (3)$$

The  $\text{Tr}$  operation calculates the trace of the matrix. The different choices for the resizing functions  $(\psi_{\text{data}}, \psi_{\text{FID}}, \hat{\psi}_{\text{FID}})$  and quantization functions  $(Q, \hat{Q})$  add further complexity to the FID evaluation protocol.

**Sources of variation.** There are three distinct resizing operations that need to be performed. Operation  $\psi_{\text{data}}$  down-samples the dataset images from  $(H, W) \rightarrow (\bar{H}, \bar{W})$  during data preparation stage (or in the data loading step during training). Operations  $\psi_{\text{FID}}$  and  $\hat{\psi}_{\text{FID}}$  resize real and generated images respectively from  $(\bar{H}, \bar{W}) \rightarrow (299, 299)$  during the evaluation stage, when we feed an image to the feature extractor  $\mathcal{F}$ .  $\psi_{\text{FID}}$  and  $\hat{\psi}_{\text{FID}}$  might be implemented differently as the mean  $\mu$  and covariance matrix  $\Sigma$  of real images are often provided by prior work. While these steps are seemingly trivial and different choices may even lead to imperceptible differences, this leads to variation in training pipelines and surprisingly large variations in downstream metrics. We discuss such sources of variations in image resizing and quantization next.

### 3.2. Image Resizing

Depending on the dataset and training size, the resizing operations  $\psi_{\text{FID}}$  and  $\hat{\psi}_{\text{FID}}$  in Figure 2 could be either downsampling or upsampling. Downsampling is the primary focus of this investigation, as it involves *throwing away information* and is more error-prone.

**Downsampling variants.** A central tenet in classic image processing, signal processing, graphics, and vision [18, 19, 53, 21, 40] is to blur or “prefilter” before subsampling, as a means of approximately removing the high-frequency information (thus preventing its misrepresentation downstream).

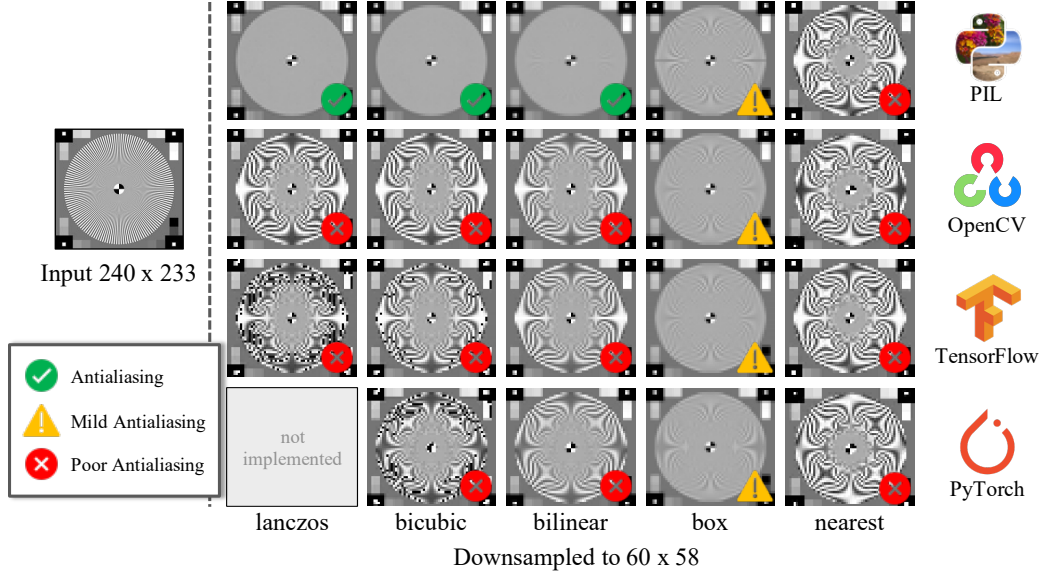


Figure 3: **Downsampling artifacts across implementations.** Qualitative results of resizing an input image by  $4\times$  using all methods provided by the commonly used image processing libraries. The high frequencies in the original image cannot be represented in the low-resolution images, and the proper downsampling method should antialias and remove such high-frequencies. Only Lanczos, bicubic, and bilinear methods implemented by PIL (top row) perform this correctly (marked in the figure with  $\checkmark$ ). All the other methods alias the high-frequency information (marked as  $\times$ ), introducing artifacts in the low-resolution image. The box filter is implemented correctly by all the libraries. However, it is a weak filter (marked as  $\triangle$ ) and does not provide sufficient antialiasing.

Different filters have subtle tradeoffs in their runtime and behavioral characteristics:

- **nearest** is using the most naive approach of subsampling every  $N$ -th element and often leads to aliasing – the high-frequency information in the original image becomes misrepresented in the downsampled image. Incorrectly implemented filters inadvertently resemble this naive approach.
- **box** is the simplest linear filter; while better than naive subsampling above, it is typically not used.
- **bilinear** and **lanczos** are increasingly powerful *linear* filters (with increasing runtime) and used more often.
- **bicubic** is nonlinear filter that provides sharper edges, with drawbacks being higher runtime and possible out-of-range values.

The top row of Figure 1 illustrates several filters (implemented by **PIL**) applied to downsampling a sparse image of a circle. Using any of these filters provides a reasonable representation of the original input circle, even when severely downsampled. Surprisingly, while these results look similar visually, the subtle differences are enough to make FID computation non-comparable, if different pre-processing is used. Secondly, most common libraries implement these operations incorrectly, as explored below.

**Implementations.** The definitions of downsampling functions are mathematical and *should never be a function of the*

*library being used*. Unfortunately, implementations differ across commonly-used libraries. We describe the libraries and functions we investigate.

- **Pillow Image Library (PIL) v8.0.1 [11]:** We use the standard `Image.resize` function; the library provides consistently antialiased results across filters.
- **OpenCV v3.4.2 [7]:** We use the standard `cv2.resize` function.
- **TensorFlow (TF) v2.0 [1]:** For the comparisons in this section we use the flags used by the original TensorFlow implementation of FID. The TensorFlow library has changed substantially through the versions. In this work we use the new TensorFlow version 2.0.
- **PyTorch v1.3.1 [43]:** We use the differentiable function `F.interpolate` on data tensors.\* This resizing method has been used by popular PyTorch implementations of FID [50].

**Buggy implementations.** In Figure 1, we show that downsampling a simple image of a circle provides wildly inconsistent results across different libraries. The **OpenCV**, **TensorFlow** and **PyTorch** implementations introduce severe aliasing artifacts. The sparse input image illustrates that the

\*A separate function, `torchvision.transforms.Resize`, is a wrapper around the PIL library and is often used in the data pre-processing step.





Figure 4: **Effects of JPEG compression on an image.** We show a sample image from the FFHQ dataset [28] that is saved with different JPEG compression ratios. Images are perceptually indistinguishable from each other but have a large FID score. The FID scores under the images are calculated between all FFHQ images saved using the corresponding JPEG format and the PNG format.

implementations do not properly blur, resulting in a disconnected set of dots after downsampling, a poor representation of the input image. The **PIL** implementation produces a connected ring. In Figure 3, we further evaluate the libraries with an image containing signals of different spatial frequencies, including the weaker **box** filter and naive **nearest**. Interestingly, the buggy implementations actually resemble the naive **nearest** method. The **box** filter is correctly implemented across libraries. However, the box filter is a weak filter and typically used only for computationally-limited scenarios.

### 3.3. Quantization and Image Compression

**Quantization.** While images are represented by 8-bit integers  $\mathbb{Z}$ , operations such as resizing and data augmentation, as well as the raw generator output will provide floating point numbers  $\mathbb{R}$ . Post-processing the results introduces more subtleties and affects standard metrics such as FID. Most simply, an image can be quantized by clipping the output between  $[0, 255]$  and rounding to produce integers. This is a lossy step and only done in instances in the pipeline when images should be saved. Additionally, we observe that performing this step has a minor effect on the FID score ( $< 0.01$ ).

**Image compression.** Saving the image as a raw matrix of values is data-intensive. However, an image contains redundant information that can be exploited. For example, the PNG format compresses an image losslessly. To further save memory, images are commonly saved using the JPEG format, with an adjustable quality score to trade-off between reducing memory and fidelity to the original. Note that JPEG compression actually varies across libraries, which has been exploited for image forensics applications [2, 3]. In Figure 4, we show a real image sampled from the FFHQ dataset [28], saved as JPEG image with the quality flag set to 100, 90, and 75 (left to right). Despite being perceptually indistinguishable (with high PSNR values of 49.3, 43.7, 39.0), the images represent a high FID scores of 0.23, 6.08 and 20.96 respectively. Note that variations across recent methods are typically  $< 1$  FID on FFHQ. FID scores are

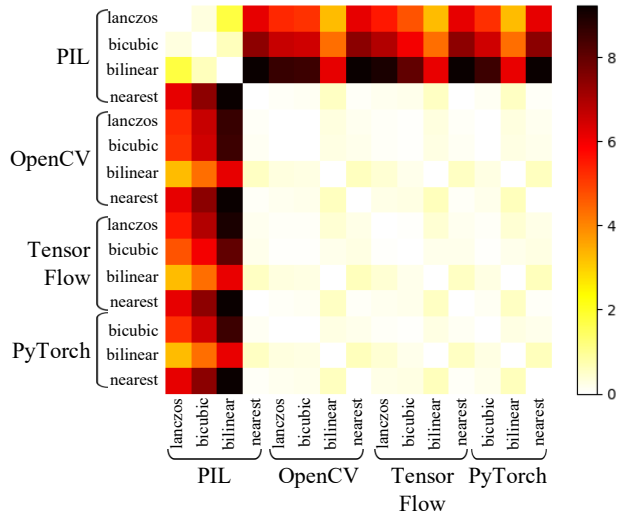


Figure 5: **FID differences caused by different downsampling methods.** Pairwise FID evaluation of inconsistencies caused by resizing methods applied to real images. The value at row  $i$  and column  $j$  in the heatmap represent the FID score obtained by comparing real FFHQ images that are resized from  $(1024, 1024)$  to  $(299, 299)$  separately by methods at index  $i$  and index  $j$  (labeled along the axes).

evaluated using 50k real images in the dataset with different JPEG compression ratios.

## 4. Experiments

In Section 3, we outlined the various image processing steps involved in FID calculation. In this section, we introduce sources of variation at these steps and quantify the resulting changes in the FID score.

In Section 4.1, we vary the procedure for FID resize function  $\psi_{\text{FID}}$  and compare the difference in FID induced. In Section 4.2, we compress images using different protocols. In Section 4.3, we evaluate the sensitivity of the FID score to different data resizing functions  $\psi_{\text{data}}$ . We then show how model selection can be affected by different FID protocols in Section 4.4. Section 4.5 explores how these image processing differences generalize beyond the FID metric. All the experiments mentioned above are done using the FFHQ dataset [28] that consists of  $1024 \times 1024$  portraits. Additionally, in Section 4.2, we additionally compare the FID differences on the LSUN outdoor Churches dataset [55], which consists of lower resolution  $(256 \times 256)$  JPEG-75 images.

### 4.1. Variation in FID Resizing Protocol ( $\hat{\psi}_{\text{FID}}$ )

Here we investigate the effects of different resizing methods in the  $\psi_{\text{FID}}$  step of FID calculation. In Table 1 (left), we begin by resizing all real dataset images from  $(1024, 1024)$  to  $(229, 229)$  using different libraries and comparing to the *same set of real images* resized with the correctly imple-

Library – filter ( $\psi_{\text{FID}}$ )	Anti-aliasing?	PIL–bicubic(Real Images) vs.			
		$\hat{\psi}_{\text{FID}}(\text{Real Images})$			$\hat{\psi}_{\text{FID}}(\text{StyleGAN2})$
		FID ↓	KID $\times 10^3$ ↓	PSNR [db] ↑	FID ↓
PIL – bicubic	✓	–	–	–	2.98
PIL – Lanczos	✓	0.30	0.27	49.6	3.16
PIL – bilinear	✓	0.64	0.65	45.6	3.98
PIL – box	⚠	0.53	0.55	45.0	3.61
OpenCV – bicubic	✗	6.51	6.50	35.7	9.81
PyTorch – bicubic	✗	6.53	6.56	35.6	9.80
TF – bicubic	✗	6.10	5.92	35.6	9.16
PIL – nearest	✗	7.43	7.60	35.1	10.77

Table 1: **Effects of different  $\hat{\psi}_{\text{FID}}$  implementations.** Different resize methods produce large inconsistencies. In the above experiments we vary the FID resizing function for images being tested  $\hat{\psi}_{\text{FID}}$  while the data resizing function  $\psi_{\text{data}}$  is the identity function and the FID resizing function for target real images  $\psi_{\text{FID}}$  is fixed as PIL–bicubic. We first show the distance on real FFHQ images [28], resized with PIL–bicubic (1024  $\rightarrow$  299) vs. other methods. PIL–Lanczos, bilinear, bicubic are correctly implemented antialiasing filters (✓); PIL–box provides mild antialiasing (⚠). These have relatively low FID scores and high PSNRs. Functions from OpenCV, PyTorch, and TensorFlow are incorrectly implemented (✗), with poor scores resembling naive nearest, which does not antialias at all. A similar trend holds on synthetic images that are generated by StyleGAN2 [29].

mented PIL bicubic. As we compare the same set of images, we would anticipate all FID scores to be close to 0 and the PSNR values to be very high. However, as shown in Figures 1 and 3, only the filters implemented by PIL are correct and visually consistent among themselves. This is reflected in Table 1 (left), where PIL Lanczos, bicubic, and box filters each have a low FID score ( $\leq 0.75$ ) and high PSNR reconstruction values ( $\geq 44$ ) to PIL bicubic. On the other hand, implementations from OpenCV, PyTorch, and TensorFlow of the same bicubic filter produce high errors (FID  $\geq 6$ , PSNR  $\sim 35$ ), resembling a naive nearest operation (FID 7.4, PSNR  $\sim 35$ ), which does not use filtering at all. Figure 5 shows a complete pairwise comparison of FID scores for all resizing methods. This is consistent with our qualitative observation (Figure 3) that OpenCV, PyTorch, and TensorFlow implement the resize operation incorrectly. Although different filters are consistent in PIL, the  $\sim 0.5$  FID indicates that differences in filtering, even though visually imperceptible, cause nontrivial variations in scores.

After studying the effects on real images, we evaluate how different resizing function  $\hat{\psi}_{\text{FID}}$  choices affect the FID score when used in a full generative modeling pipeline. We consider the case where no downsampling occurs in the data ( $\psi_{\text{data}}$  is identity function) but severe downsampling occurs in the FID calculation steps  $\psi_{\text{FID}}$  and  $\hat{\psi}_{\text{FID}}$ . We use a pretrained StyleGAN2 generator [29] trained on 1024  $\times$  1024 FFHQ images. We generate 50,000 images using the model and process them separately, before passing them to the InceptionV3 network [52]. In Table 1 (right), we resize the same

Image Format ( $\hat{Q}$ )	$Q(\text{Real Images})$ vs.			
	$\hat{Q}(\text{Real Images})$			$\hat{Q}(\text{StyleGAN2})$
	FID ↓	KID $\times 10^3$ ↓	PSNR [db] ↑	FID ↓
PNG	–	–	–	3.03
JPEG-100	0.23	0.12	49.3	3.11
JPEG-98	0.29	0.17	46.3	3.29
JPEG-95	1.39	1.40	43.6	4.86
JPEG-90	6.08	6.88	41.7	10.39
JPEG-75 <sup>†</sup>	20.96	24.64	38.9	25.87

Table 2: **Effects of JPEG compression during FID calculation.** The images are resized from 1024 to 299 using PIL with bicubic filter and subsequently compressed using the JPEG format with different quality flags. Each row compares the FID score between images saved with a particular image format and the same images saved using the lossless PNG format. JPEG compression does not degrade the images perceptually (the default PIL setting is marked by <sup>†</sup>), as seen by a relatively small decrease in the PSNR value but results in a steep increase in the FID score. The table on the left compares real images from the FFHQ [28] dataset to the same set of images stored differently. In contrast, the table on the right evaluates the images generated by StyleGAN2 [29].

output of the generator from (1024  $\times$  1024) to (299  $\times$  299) using different options and compare to real images from the dataset that are resized using the PIL library and the bicubic filter. We observe that the effect of different resizing options in  $\hat{\psi}_{\text{FID}}$  on StyleGAN2 generated images shown in Table 1 (right) is similar to the effect on real images shown in Table 1 (left). For example, using PIL bicubic downsampling gives 2.98 FID, while buggy bicubic implementations give values between 9–10, close to using naive nearest (10.77). Even using the correctly implemented PIL bilinear raises the score from 2.98 (when PIL bicubic is used) to 3.98.

#### 4.2. Quantization / Compression after FID Resizing

In Table 2, we show a similar test across quantization methods applied to real FFHQ images (left) and StyleGAN2 generated images (right). For the real images, the FID and PSNR scores are computed between the uncompressed PNG images and JPEG-compressed images. When saving using the JPEG-100, which is the highest quality, there is still some information loss that results in 0.23 FID. The PIL default value of JPEG-75 gives perceptually close results (PSNR 38.9). However, the FID is at 20.96, substantially higher than state-of-the-art generation methods [29] (FID 2.84). This indicates that in data processing pipelines, a seemingly innocuous operation such as saving as JPEG (even with default parameters) can dramatically change the metrics. We observe an analogous trend when we perform this test on StyleGAN2 generated images in Table 2 (right). JPEG-100 compression of the images increase the FID score slightly from 3.03 to 3.11, whereas the default JPEG-75 compression

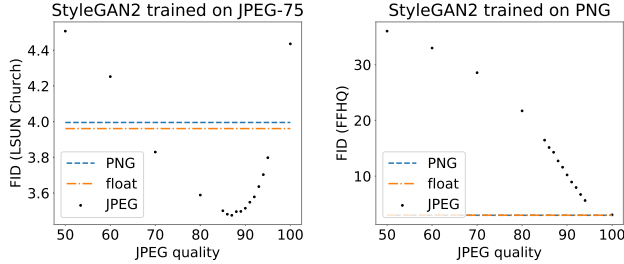


Figure 6: **Effects of image quantization / compression on FID.** We vary the format used for storing the generated images and plot the resulting changes in the FID of a StyleGAN2 model [29] trained on the FFHQ dataset [28] (left) and LSUN outdoor Church dataset [55] (right). The images generated by the StyleGAN2 are resized  $1024 \rightarrow 299$  using PIL-bicubic and stored using different formats before computing the FID score. Note that LSUN dataset images were collected with JPEG compression (quality 75), whereas FFHQ images were collected as PNG. The blue dashed line in both graphs shows the FID score when the generated images are quantized to 8-bit unsigned integers (PNG). Whereas the orange dashed line shows the FID score if the generated images are left unquantized as floating-point numbers.

Data downsampling $\psi_{\text{data}}$	FID $\downarrow$ (PIL-bicubic)
PIL – bilinear	9.00
PIL – Lanczos	7.71
PyTorch – bilinear	6.76

Table 3: **Effects of different  $\psi_{\text{data}}$  implementations.** We vary the dataset preprocessing resize function  $\psi_{\text{data}}$  while the other resizing functions  $\hat{\psi}_{\text{FID}}$  and  $\psi_{\text{FID}}$  are correctly implemented as PIL-bicubic. FID Comparison of different StyleGAN2 [29] (config-e) models trained with an identical training procedure, but with FFHQ images pre-processed from 1024 to 256 differently. Note that using a buggy resizing function (PyTorch bilinear) to pre-process the images actually produces an easier-to-model distribution.

increases the FID score to 25.87.

In both of the comparisons, each method was compared with the FFHQ dataset images, which were collected as uncompressed PNG files. Any additional compression only monotonically increases the FID score (Figure 6 right). This does not apply to other datasets which were collected as JPEG images. To study this effect, we train a StyleGAN2 model [29] on the LSUN outdoor Church dataset [55] that was collected as JPEG-75 images. In Figure 6 (left), we plot the FID of the trained generator as the generated images are quantized and compressed differently. We observe that the FID score for the StyleGAN2 model trained on LSUN outdoor Church images *improves when slight JPEG compression is added*. The best FID score (3.48) is obtained when the generated images are compressed with JPEG quality 87. (The FID score for the generated images stores as PNG files is 4.00). Following these observations, we recommend that researchers curate and store training images as PNG formats for the future GAN datasets.

### 4.3. Variation in Data Resizing Protocol ( $\psi_{\text{data}}$ )

Previously, we considered the scenario when the dataset was not downsampled (i.e.,  $\psi_{\text{data}}$  is the identity function). However, as discussed in Section 1 and illustrated in Figure 2, a common practice among research community is training a model on a low-res version of the original dataset [59, 27, 57]. Researchers need to pre-process the dataset images beforehand to the desired lower resolution (e.g.,  $256 \times 256$  for FFHQ or  $128 \times 128$  for ImageNet) or pre-process a batch of images during data loading. Before, the target distribution was fixed, and differences were purely introduced during post-hoc FID evaluation. Now, the situation is much more complicated. *Different resizing choices will result in different training distributions entirely.* In this section, we study the effects of resizing the dataset images using separate implementations.

In Table 3, we train three different StyleGAN2 [29] (config-e) models following an identical procedure (official PyTorch implementation<sup>†</sup> for 10k iterations) on FFHQ [28], with images that are resized to  $256 \times 256$  using PIL Lanczos, PIL bilinear, and PyTorch bilinear filters. Note the the resizing functions  $\psi_{\text{FID}}$  and  $\hat{\psi}_{\text{FID}}$  ( $256 \rightarrow 299$ ) are *upsampling* functions implemented with PIL bicubic. Here, interestingly, we observe that that the buggy PyTorch bilinear pre-processing results in *lower* FID values. This indicates that unintuitively, using an incorrect pre-processing procedure can actually provide an easier-to-model distribution and an unfair advantage over researchers who use correct resizing functions.

### 4.4. Model Selection

Thus far, we have established that OpenCV, TensorFlow, and Pytorch implementations are incorrect. These libraries are commonly used by default, and we refer to these implementations as **FID-buggy**. We refer to PIL bicubic as **FID-correct**. In this section, we consider two cases in particular. We first compare the difference across different generative models that are each trained to completion using the same dataset. Following that we compare the differences across different intermediate checkpoints of a single training run for a generative model.

**Comparison across different models.** We analyse how the relative difference between different generative models is affected by using different resizing implementations. In particular, we evaluate the different configurations of StyleGAN2 [29], StyleGAN [28], and MSG-GAN [25] trained to generate  $1024 \times 1024$  FFHQ images [28] and show scores in Table 4. While the general trend is the same across different models for different FID scores, indicating that the relative model ordering between these papers is accurate, *the relative improvement is not consistent*. Note that the

<sup>†</sup><https://github.com/NVlabs/stylegan2-ada>

Model	FID↓ ( $\Delta$ from StyleGAN2-f)		
	TensorFlow (✗)	Pytorch (✗)	PIL (✓)
StyleGAN2 (f)	2.76 (0.00)	2.69 (0.00)	2.98 (0.00)
StyleGAN2 (e)	3.22 (0.46)	3.10 (0.41)	3.69 (0.71)
StyleGAN2 (d)	4.25 (1.49)	4.15 (1.46)	4.68 (1.70)
StyleGAN2 (c)	4.38 (1.62)	4.28 (1.59)	4.74 (1.76)
StyleGAN2 (b)	4.27 (1.51)	4.15 (1.46)	4.69 (1.71)
StyleGAN	4.39 (1.63)	4.29 (1.60)	4.74 (1.76)
MSG-GAN	6.00 (3.24)	5.94 (3.25)	6.51 (3.53)

Table 4: **Relative difference in FID across different models under different  $\psi_{\text{FID}}$ .** A set of 50,000 images generated by different models and evaluated with different FID protocols. Each FID entry (row) is computed using same set of images generated by corresponding StyleGAN2 [29] variants and MSG-GAN [25] model. The **value in parenthesis** shows the relative difference in the corresponding FID score from StyleGAN2 config-F (top row). Note that the difference between config-F and config-E is obscured when using a buggy resize function vs. a correctly implemented one.

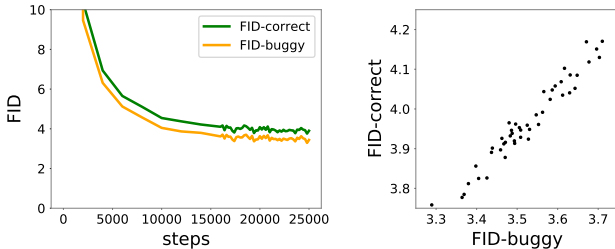


Figure 7: **Evaluating across checkpoints.** Comparison across different intermediate checkpoints while training a StyleGAN2 model [29] on the FFHQ dataset [28] using FID-buggy and FID-correct. The scatter plot on the right shows that the relationship between the two metrics is not strictly monotonic.

variation in FID values is similar across all three implementations (0.644, 0.637, 0.681 amongst StyleGAN2 variants for FID-official, FID-buggy, and FID-correct, respectively), indicating that the deviations of scores across variants of a model is on the same scale. Even so, the improvement from StyleGAN2 config-E and config-F is 0.46 and 0.41 between FID-official and FID-buggy, but is much larger (0.71) when evaluated with the correct resizing implementation. As config-F takes increased computational resources, this may affect the choice of downstream users considering the cost-performance tradeoff between these two models.

**Comparison across checkpoints.** We train a StyleGAN2 generator [29] (config-e) and evaluate different intermediate checkpoints. In Figure 7, the graph (left) plots FID-buggy and FID-correct at different stages in the training. The scatter plot (right) directly compares the two FID scores. We note that the two FID scores are not 100% correlated and that an improvement in the buggy FID does not always translate to an analogous improvement in the correct FID.

## 4.5. Generalizing Beyond FID

In previous sections, we have shown that incorrectly implemented image processing can change the FID score. This difference exists due to a change in the distribution of image features that are extracted by the pretrained Inception network [52]. Generative evaluation metrics other than FID also use the same Inception network. Subsequently, we show that the KID score [5] is similarly sensitive to incorrect image resizing and image compression in Table 1 and Table 2 respectively. We compare the KID score differences on FFHQ [28] images resized with PIL-bicubic vs. other methods. In Table 1, we show that PIL Lanczos, bicubic, and box filters each have a low KID score ( $\leq 0.7 \times 10^3$ ). However the same bicubic filter’s implementation from OpenCV, PyTorch, and TensorFlow produce a high KID score ( $\geq 5 \times 10^3$ ) resembling the naive nearest operation ( $7.60 \times 10^3$ ). In Table 2, we observe that even compressing with the highest quality (JPEG-100) results in some information loss ( $0.12 \times 10^3$  KID). Reducing the quality further and using the PIL default of JPEG-75 increases the difference to  $24.64 \times 10^3$  KID.

## 5. Recommendations

Thus far, we have shown surprisingly large sensitivities to seemingly inconsequential implementation details. Based on our observations, we discuss some best practices when training a generative model and computing the corresponding FID scores. We split into two cases: model training at the native dataset resolution ( $1024 \times 1024$  for FFHQ [28] dataset), and model training at a reduced resolution ( $256 \times 256$ ).

For training a model at the native resolution, two resize operations need to get performed:  $\psi_{\text{FID}}$  for real images, and  $\hat{\psi}_{\text{FID}}$  for generated images. Based on the qualitative results shown in Figure 1, Figure 3 and the quantitative results shown in Section 4.1 and Section 4.2, we recommend using the **bicubic** method implemented by the **PIL** library for both.

When training a model at a lower resolution, three resize operations  $\psi_{\text{data}}$ ,  $\psi_{\text{FID}}$ , and  $\hat{\psi}_{\text{FID}}$  are involved. Following the conclusions in Section 4.3, we recommend using **PIL - bicubic** method for all three operations and only comparing against other methods that use the same resizing method implemented by the same library. In cases where the dataset comprises uncompressed PNG images, we caution against the use of JPEG compression even at the highest quality.

There are many details one needs to keep track of when computing the FID score. Any inconsistency in the steps leads to results that are no longer comparable to other methods. The resize operation and the image quantization/compression are especially impactful. To facilitate an easy comparison, avoid inconsistent comparisons, and encourage the usage of critical operations that are correctly implemented, we provide an easy-to-use library, clean-fid, at [github.com/GaParmar/clean-fid](https://github.com/GaParmar/clean-fid). In addition, we provide pre-computed Inception features [52] for standard benchmarks at various resolutions.



**Acknowledgments.** We thank Jaakko Lehtinen and Assaf Shocher for bringing attention to this issue and for helpful discussion. We thank Sheng-Yu Wang, Nupur Kumari, Kangle Deng, and Andrew Liu for useful discussions. We thank William S. Peebles, Shengyu Zhao, and Taesung Park for proofreading our manuscript. We are grateful for the support of Adobe, Naver Corporation, and Sony Corporation.

## References

- [1] Martín Abadi, Paul Barham, Jianmin Chen, Zhifeng Chen, Andy Davis, Jeffrey Dean, Matthieu Devin, Sanjay Ghemawat, Geoffrey Irving, Michael Isard, et al. Tensorflow: A system for large-scale machine learning. In *12th {USENIX} symposium on operating systems design and implementation ({OSDI} 16)*, pages 265–283, 2016. 4
- [2] Shruti Agarwal and Hany Farid. Photo forensics from jpeg dimples. In *2017 IEEE Workshop on Information Forensics and Security (WIFS)*, 2017. 5
- [3] Shruti Agarwal and Hany Farid. Photo forensics from rounding artifacts. In *Proceedings of the 2020 ACM Workshop on Information Hiding and Multimedia Security*, pages 103–114, 2020. 5
- [4] Sanjeev Arora and Yi Zhang. Do gans actually learn the distribution? an empirical study. In *International Conference on Learning Representations (ICLR)*, 2018. 2
- [5] Mikolaj Bińkowski, Dougal J Sutherland, Michael Arbel, and Arthur Gretton. Demystifying mmd gans. In *ICLR*, 2018. 2, 8
- [6] Ali Borji. Pros and cons of gan evaluation measures. *Computer Vision and Image Understanding*, 179:41–65, 2019. 2
- [7] Gary Bradski and Adrian Kaehler. Opencv. *Dr. Dobbs's journal of software tools*, 3, 2000. 4
- [8] Andrew Brock, Jeff Donahue, and Karen Simonyan. Large scale gan training for high fidelity natural image synthesis. In *International Conference on Learning Representations (ICLR)*, 2019. 1
- [9] Andrew Brock, Jeff Donahue, and Karen Simonyan. Large scale gan training for high fidelity natural image synthesis. In *International Conference on Learning Representations (ICLR)*, 2019. 2
- [10] Min Jin Chong and David Forsyth. Effectively unbiased fid and inception score and where to find them. In *CVPR*, 2020. 2
- [11] Alex Clark. Pillow (pil fork) documentation, 2015. 4
- [12] Jia Deng, Wei Dong, Richard Socher, Li-Jia Li, Kai Li, and Li Fei-Fei. Imagenet: A large-scale hierarchical image database. In *IEEE Conference on Computer Vision and Pattern Recognition (CVPR)*, 2009. 3, 11
- [13] Emily L Denton, Soumith Chintala, Rob Fergus, et al. Deep generative image models using a laplacian pyramid of adversarial networks. In *Advances in Neural Information Processing Systems*, 2015. 2
- [14] Laurent Dinh, Jascha Sohl-Dickstein, and Samy Bengio. Density estimation using real nvp. In *International Conference on Learning Representations (ICLR)*, 2017. 2
- [15] Jeff Donahue and Karen Simonyan. Large scale adversarial representation learning. In *Advances in Neural Information Processing Systems*, 2019. 2
- [16] Alexey Dosovitskiy and Thomas Brox. Generating images with perceptual similarity metrics based on deep networks. In *Advances in Neural Information Processing Systems*, 2016. 3
- [17] Yilun Du and Igor Mordatch. Implicit generation and generalization in energy-based models. In *Advances in Neural Information Processing Systems*, 2019. 2
- [18] James D Foley, Andries Van Dam, Steven K Feiner, John F Hughes, and Richard L Phillips. *Introduction to computer graphics*, volume 55. Addison-Wesley Reading, 1994. 3
- [19] David A Forsyth and Jean Ponce. *Computer vision: a modern approach*. Pearson,, 2012. 3
- [20] Leon A Gatys, Alexander S Ecker, and Matthias Bethge. Image style transfer using convolutional neural networks. In *IEEE Conference on Computer Vision and Pattern Recognition (CVPR)*, 2016. 3
- [21] Rafael C Gonzalez, Richard E Woods, et al. Digital image processing, 2002. 3
- [22] Ian Goodfellow, Jean Pouget-Abadie, Mehdi Mirza, Bing Xu, David Warde-Farley, Sherjil Ozair, Aaron Courville, and Yoshua Bengio. Generative adversarial nets. In *Advances in Neural Information Processing Systems*, 2014. 2
- [23] Martin Heusel, Hubert Ramsauer, Thomas Unterthiner, Bernhard Nessler, and Sepp Hochreiter. GANs trained by a two time-scale update rule converge to a local Nash equilibrium. In *Advances in Neural Information Processing Systems*, 2017. 1, 2
- [24] Justin Johnson, Alexandre Alahi, and Li Fei-Fei. Perceptual losses for real-time style transfer and super-resolution. In *European Conference on Computer Vision (ECCV)*, 2016. 3
- [25] Animesh Karnewar and Oliver Wang. Msg-gan: Multi-scale gradients for generative adversarial networks. In *IEEE Conference on Computer Vision and Pattern Recognition (CVPR)*, 2020. 7, 8
- [26] Tero Karras, Timo Aila, Samuli Laine, and Jaakko Lehtinen. Progressive growing of gans for improved quality, stability, and variation. In *International Conference on Learning Representations (ICLR)*, 2018. 2
- [27] Tero Karras, Miika Aittala, Janne Hellsten, Samuli Laine, Jaakko Lehtinen, and Timo Aila. Training generative adversarial networks with limited data. *NIPS*, 33, 2020. 7
- [28] Tero Karras, Samuli Laine, and Timo Aila. A style-based generator architecture for generative adversarial networks. In *IEEE Conference on Computer Vision and Pattern Recognition (CVPR)*, 2019. 1, 2, 5, 6, 7, 8, 11
- [29] Tero Karras, Samuli Laine, Miika Aittala, Janne Hellsten, Jaakko Lehtinen, and Timo Aila. Analyzing and improving the image quality of stylegan. *IEEE Conference on Computer Vision and Pattern Recognition (CVPR)*, 2020. 6, 7, 8
- [30] Diederik P Kingma and Prafulla Dhariwal. Glow: Generative flow with invertible 1x1 convolutions. In *Advances in Neural Information Processing Systems*, 2018. 1, 2
- [31] Diederik P Kingma and Max Welling. Auto-encoding variational bayes. *International Conference on Learning Representations (ICLR)*, 2014. 2

- [32] Tuomas Kynkäänniemi, Tero Karras, Samuli Laine, Jaakko Lehtinen, and Timo Aila. Improved precision and recall metric for assessing generative models. In *Advances in Neural Information Processing Systems*, 2019. 2
- [33] Erich L Lehmann and Joseph P Romano. *Testing statistical hypotheses*. Springer Science & Business Media, 2006. 2
- [34] Ming-Yu Liu, Xun Huang, Arun Mallya, Tero Karras, Timo Aila, Jaakko Lehtinen, and Jan Kautz. Few-shot unsupervised image-to-image translation. In *IEEE International Conference on Computer Vision (ICCV)*, 2019. 2
- [35] Steven Liu, Tongzhou Wang, David Bau, Jun-Yan Zhu, and Antonio Torralba. Diverse image generation via self-conditioned gans. In *IEEE Conference on Computer Vision and Pattern Recognition (CVPR)*, 2020. 2
- [36] David Lopez-Paz and Maxime Oquab. Revisiting classifier two-sample tests. In *ICLR*, 2017. 2
- [37] Mario Lucic, Karol Kurach, Marcin Michalski, Sylvain Gelly, and Olivier Bousquet. Are gans created equal? a large-scale study. In *Advances in Neural Information Processing Systems*, 2018. 2
- [38] Erik Nijkamp, Mitch Hill, Tian Han, Song-Chun Zhu, and Ying Nian Wu. On the anatomy of mcmc-based maximum likelihood learning of energy-based models. In *AAAI Conference on Artificial Intelligence (AAAI)*, 2020. 2
- [39] Aaron van den Oord, Nal Kalchbrenner, Oriol Vinyals, Lasse Espeholt, Alex Graves, and Koray Kavukcuoglu. Conditional image generation with pixelcnn decoders. In *Advances in Neural Information Processing Systems*, 2016. 2
- [40] Alan V Oppenheim. *Discrete-time signal processing*. Pearson Education India, 1999. 3
- [41] Taesung Park, Ming-Yu Liu, Ting-Chun Wang, and Jun-Yan Zhu. Semantic image synthesis with spatially-adaptive normalization. In *IEEE Conference on Computer Vision and Pattern Recognition (CVPR)*, 2019. 2
- [42] Gaurav Parmar, Dacheng Li, Kwonjoon Lee, and Zhuowen Tu. Dual contradistinctive generative autoencoder. In *IEEE Conference on Computer Vision and Pattern Recognition (CVPR)*, 2021. 2
- [43] Adam Paszke, Sam Gross, Francisco Massa, Adam Lerer, James Bradbury, Gregory Chanan, Trevor Killeen, Zeming Lin, Natalia Gimelshein, Luca Antiga, et al. Pytorch: An imperative style, high-performance deep learning library. In *Advances in Neural Information Processing Systems*, 2019. 4
- [44] Alec Radford, Luke Metz, and Soumith Chintala. Unsupervised representation learning with deep convolutional generative adversarial networks. In *International Conference on Learning Representations (ICLR)*, 2016. 2
- [45] Suman Ravuri and Oriol Vinyals. Classification accuracy score for conditional generative models. In *Advances in Neural Information Processing Systems*, 2019. 2
- [46] Ali Razavi, Aaron van den Oord, and Oriol Vinyals. Generating diverse high-fidelity images with vq-vae-2. In *NIPS*, 2019. 1, 2
- [47] Mehdi SM Sajjadi, Olivier Bachem, Mario Lucic, Olivier Bousquet, and Sylvain Gelly. Assessing generative models via precision and recall. In *Advances in Neural Information Processing Systems*, 2018. 2
- [48] Ruslan Salakhutdinov and Geoffrey Hinton. Deep boltzmann machines. In *Artificial intelligence and statistics*, pages 448–455, 2009. 2
- [49] Tim Salimans, Ian Goodfellow, Wojciech Zaremba, Vicki Cheung, Alec Radford, and Xi Chen. Improved techniques for training gans. In *Advances in Neural Information Processing Systems*, 2016. 2
- [50] Maximilian Seitzer. pytorch-fid: FID Score for PyTorch. <https://github.com/mseitzer/pytorch-fid>, August 2020. Version 0.1.1. 4
- [51] Ashish Shrivastava, Tomas Pfister, Oncel Tuzel, Josh Susskind, Wenda Wang, and Russ Webb. Learning from simulated and unsupervised images through adversarial training. In *IEEE Conference on Computer Vision and Pattern Recognition (CVPR)*, 2017. 2
- [52] Christian Szegedy, Vincent Vanhoucke, Sergey Ioffe, Jon Shlens, and Zbigniew Wojna. Rethinking the inception architecture for computer vision. In *IEEE Conference on Computer Vision and Pattern Recognition (CVPR)*, 2016. 3, 6, 8
- [53] Richard Szeliski. *Computer vision: algorithms and applications*. Springer Science & Business Media, 2010. 3
- [54] Lucas Theis, Aäron van den Oord, and Matthias Bethge. A note on the evaluation of generative models. In *ICLR*, 2016. 2
- [55] Fisher Yu, Yinda Zhang, Shuran Song, Ari Seff, and Jianxiong Xiao. Lsun: Construction of a large-scale image dataset using deep learning with humans in the loop. *arXiv preprint arXiv:1506.03365*, 2015. 5, 7, 11
- [56] Han Zhang, Zizhao Zhang, Augustus Odena, and Honglak Lee. Consistency regularization for generative adversarial networks. In *International Conference on Learning Representations (ICLR)*, 2020. 2
- [57] Han Zhang, Zizhao Zhang, Augustus Odena, and Honglak Lee. Consistency regularization for generative adversarial networks. In *International Conference on Learning Representations (ICLR)*, 2020. 2, 7
- [58] Richard Zhang, Phillip Isola, Alexei A Efros, Eli Shechtman, and Oliver Wang. The unreasonable effectiveness of deep features as a perceptual metric. In *IEEE Conference on Computer Vision and Pattern Recognition (CVPR)*, 2018. 1, 3
- [59] Shengyu Zhao, Zhijian Liu, Ji Lin, Jun-Yan Zhu, and Song Han. Differentiable augmentation for data-efficient gan training. In *Advances in Neural Information Processing Systems (NeurIPS)*, 2020. 2, 7
- [60] Sharon Zhou, Mitchell L Gordon, Ranjay Krishna, Austin Narcomey, Li Fei-Fei, and Michael S Bernstein. Hype: A benchmark for human eye perceptual evaluation of generative models. In *Advances in Neural Information Processing Systems*, 2019. 2
- [61] Jun-Yan Zhu, Philipp Krähenbühl, Eli Shechtman, and Alexei A Efros. Generative visual manipulation on the natural image manifold. In *European Conference on Computer Vision (ECCV)*, 2016. 2

Library – filter ( $\hat{\psi}_{\text{FID}}$ )	LSUN Outdoor Churches			ImageNet		
	PIL-bicubic Vs. $\hat{\psi}_{\text{FID}}$			PIL-bicubic Vs. $\hat{\psi}_{\text{FID}}$		
	FID ↓	KID $\times 10^3$ ↓	PSNR ↑	FID ↓	KID $\times 10^3$ ↓	PSNR ↑
PIL – bicubic	–	–	–	–	–	–
PIL – Lanczos	0.062	0.04	36.1	0.047	0.00	45.9
PIL – bilinear	0.164	0.11	40.0	0.134	0.00	42.2
PIL – box	1.521	1.39	29.5	0.458	0.02	35.8
OpenCV – bicubic	0.040	0.02	37.3	0.393	0.02	36.1
PyTorch – bicubic	0.063	0.06	40.0	0.392	0.02	36.1
TF – bicubic	0.015	0.00	40.0	0.346	0.02	37.0
PIL – nearest	1.519	1.40	29.5	1.947	0.10	31.0

Table 5: **Effects of different resizing  $\hat{\psi}_{\text{FID}}$  implementations on additional datasets.** Different resize methods produce different amounts of inconsistencies on different datasets. In the experiments shown above, we vary the FID resizing function for the set of images being tested  $\hat{\psi}_{\text{FID}}$ , while the FID resizing function for reference images  $\psi_{\text{FID}}$  is fixed as PIL-bicubic. On the left, we show that the incorrectly implemented bicubic methods have a minimal effect on the FID score ( $\sim 0.05$ ) on the LSUN Outdoor Churches [55] dataset images ( $256 \rightarrow 299$ ). On the right, we show that these filters have a slightly more prominent effect on the FID score ( $\sim 0.4$ ) when evaluated on the ImageNet dataset. Note that the differences for both of these datasets are much more minor than the difference on FFHQ dataset images ( $\sim 6.5$ ) shown in Table 1.

## 6. Appendix

### 6.1. Evaluating Additional Datasets.

As shown in Table 1, the different implementation choices for the three resizing functions  $\psi_{\text{data}}$ ,  $\psi_{\text{FID}}$ ,  $\hat{\psi}_{\text{FID}}$  can change the FID metric computed on the FFHQ dataset [28] images. In this section, we investigate if similar differences are found when resizing images from other commonly used datasets.

We begin by considering two additional datasets - LSUN Outdoor Churches [55] and ImageNet [12]. Table 5 resizes the dataset images using different methods and compares the FID, KID, and PSNR scores. We use 50,000 images for the FID and KID evaluation, whereas the PSNR is computed with 1,000 images. Surprisingly, we do not find the same trend that we observed on FFHQ images in Table 1. The FID between ImageNet images resized with PIL-bicubic and the images resized with the incorrect bicubic filter implementations from OpenCV, PyTorch, TensorFlow is  $\sim 0.4$ . This difference in the FID scores further reduces to  $< 0.07$  when considering the LSUN Outdoor Churches images. These differences are much more minor than the significant difference ( $\sim 6.5$ ) observed on FFHQ images in Table 1.

The different resizing factors can explain the different sensitivity of the FID score to resizing methods on different datasets. The LSUN Outdoor Churches dataset consists of images at resolution  $256 \times 256$ , and consequently, the resizing operations  $\psi_{\text{FID}}$  and  $\hat{\psi}_{\text{FID}}$  involve upsampling  $256 \rightarrow 299$ . The ImageNet validation set images do not have a fixed size but a majority of the images have the shorter side to be  $\sim 350$ . The incorrect bicubic implementations do not introduce significant aliasing artifacts when either upsampling or downsampling by a small amount. In contrast, the resize operations  $\psi_{\text{FID}}$  and  $\hat{\psi}_{\text{FID}}$  on FFHQ images involve downsampling

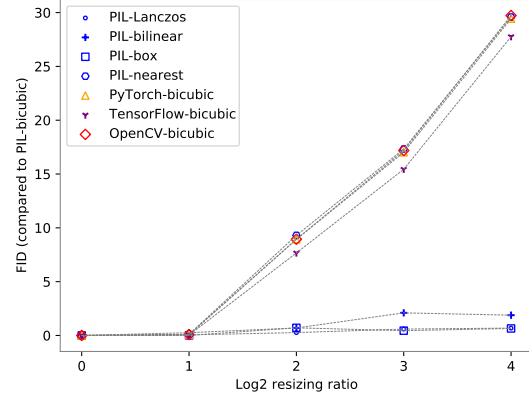


Figure 8: **Effects of different resizing ratios in the data preprocessing resize function  $\psi_{\text{data}}$ .** We resize the FFHQ dataset [28] images ( $1024 \rightarrow 299$ ) following a two-step process. For a resizing ratio  $r$ , the images are first resized ( $1024 \rightarrow \frac{1024}{r}$ ) using the resizing implementation being tested  $\psi_{\text{data}}$  and subsequently resized ( $\frac{1024}{r} \rightarrow 299$ ) using PIL-bicubic. The plot shows the FID score computed between images resized with PIL-bicubic in the initial resizing step  $\psi_{\text{data}}$  and the corresponding resizing implementation being tested. The implementation of the bicubic filters from PyTorch, TensorFlow, and OpenCV properly antialias the input when the downsampling ratio is less than 2 - increasing the resizing ratio beyond this threshold introduces an increasing amount of aliasing artifacts.

with a much larger resizing factor ( $1024 \rightarrow 299$ ).

### 6.2. Resizing Factor

Here, we further study whether the resizing factor (the ratio of input image size to the output image size) affects the FID scores for correctly implemented PIL-bicubic filter and incorrectly implemented filters by other libraries.

Figure 8 shows how the artifacts introduced by the incorrect resizing methods vary as the resizing ratio is varied. To evaluate a resizing method for a ratio  $r$ , we resize the FFHQ dataset [28] images using a two-step process. First, we resize the dataset images  $1024 \rightarrow \frac{1024}{r}$  using the method being tested. We then resize these images  $\frac{1024}{r} \rightarrow 299$  with PIL-bicubic. Following the two-step resizing process, we compare the images to reference images generated using PIL-bicubic for both of the resizing steps. We observe from the results that a downsampling ratio  $r$  of less than 2 has a small corresponding FID score for all the resizing methods. However, increasing the resizing ratio beyond this threshold results in a steep increase in the FID score.